Saturation in Cascaded Optical Amplifier Free-Space Optical Communication Systems

O. J. Bandele, P. N. Desai*, M. S. Woolfson, A. J. Phillips

Department of Electrical and Electronic Engineering, Faculty of Engineering, University of Nottingham, University Park, Nottingham, NG7 2RD, UK

*was with Faculty of Engineering, University of Nottingham, University Park, Nottingham, NG7 2RD, UK, now with Department of Electrical, Electronic Engineering and Instrumentation, BITS Pilani, Zuarinagar, Goa, 403726, India

Corresponding Author E-mail: andrew.phillips@nottingham.ac.uk

Abstract

The performance of a free-space optical (FSO) communication system in a turbulent atmosphere employing an optical amplifier (OA) cascade to extend reach is investigated. Analysis of both single and cascaded OA FSO communication links is given and the implications of using both adaptive (to channel state) and non-adaptive decision threshold schemes are analysed. The benefits of amplifier saturation, for example in the form of effective scintillation reduction when a non-adaptive decision threshold scheme is utilized at the receiver for different atmospheric turbulence regimes, are presented. Monte Carlo simulation techniques are used to model the probability distributions of the optical signal power, noise and the average bit error rate (BER) due to scintillation for the cascade. The performance of an adaptive decision threshold is superior to a non-adaptive decision threshold for both saturated and fixed gain preamplified receivers and that the ability of a saturated gain OA to suppress scintillation is only meaningful for system performance when a non-adaptive decision threshold is used at the receiver. An OA cascade can be successfully used to extend reach in FSO communication systems and specific system implementations are presented. The optimal cascade scheme with a non-adaptive receiver would use frequent low gain saturated amplification.

1 Introduction

The past three decades have witnessed the emergence of free-space optical (FSO) communication as a viable approach for terrestrial short range access networks. The catalysts for the development of the FSO communication systems are the rising demands for higher bandwidth and technological developments in optoelectronics such as sensitive detectors and high power transmitters [1-3]. The main advantages of FSO communication systems over the traditional radio frequency (RF) and millimetre wave systems include the large potential bandwidth obtainable, improved security of information and absence of spectrum licensing requirements. The employment of a FSO communication system also eliminates the cost of purchasing and laying the optical fibre which would be needed in optical fibre communication systems [4, 5]. Though FSO systems offers many advantages, their practical implementation is highly susceptible to unpredictable severe atmospheric conditions. For instance, beam attenuation can occur as a result of scattering and photon absorption which is caused by rain, fog, snow, aerosol and atmospheric gases. Also, thermal expansion, earth tremors and wind loads can result in high-rise building sway [1, 6]. Even in clear weather conditions, due to inhomogenities in pressure and temperature changes in the atmosphere, the refractice index varies leading to atmospheric turbulence. The effect of atmospheric turbulence is highly significant because it results in scintillation i.e. fluctuations of the power of the optical signal propagated through the atmosphere [2, 6, 7]. These fluctuations in the received signal power lead to a reduction in system performance. In order to achieve the desired bit error rate (BER), appropriate fade mitigation techniques should be employed [8]. Various techniques that have been proposed in the literature include aperture averaging [1, 9], error correcting codes with interleaving [10], spatial diversity [3, 7, 11, 12], cooperative diversity and multi-hop transmission [13], maximum likelihood sequence detection (MLSD) [14], and the use of a saturated optical amplifier (OA) [15-17].

While optical amplifiers (OAs) may be used in a number of configurations to extend reach or improve receiver sensitivity in optical fibre systems [18], they can also be similarly used in FSO

communication systems [2]. Unfortunately, the OA is not a perfect device as it generates optical noise in the form of amplified spontaneous emission (ASE). The ASE noise further generates beat noises known as spontaneous-spontaneous and signal-spontaneous beat noises [2, 3]. Naturally, the OA saturates at large input signals and gives reduced gain but, while it is not the usual mode of operation for an optical preamplifier, there is no fundamental reason not to operate optical preamplifiers in the saturation regime [18] and indeed this strategy may have advantages. The gain saturation process has been found useful for suppressing atmospherically induced scintillation in experimental work of Abtahi *et al* [17] and Ciaramella *et al* [19]. The ability of saturated OAs to suppress scintillation has also been theoretically shown by Yiannopoulos *et al* [15] and Boucouvalas *et al* [16] where they considered the effective fade probability. The nonlinear amplification property of a saturated semiconductor optical amplifier (SOA) was mentioned in [20] but since channel state information (CSI) was assumed known, the BER results obtained naturally were not able to show that suppressing scintillation in the absence of CSI was beneficial. The suppression of scintillation in a non-return-to-zero (NRZ) on-off keying (OOK) FSO communication link using one or more saturated OAs is considered in this work. The BER, in the presence of ASE noise, is shown for various turbulence levels, all modelled with a gamma-gamma (GG) distribution, and different threshold setting schemes are analysed.

After this introductory part, the atmospheric turbulence model used to characterise the FSO link is described in section 2. Section 3 describes a single link optically preamplified FSO receiver model. Section 4 describes the optical signal to noise ratio (OSNR) and BER analysis for a cascaded OA FSO link. The results of the numerical analysis and Monte Carlo (MC) simulations for a single and cascaded OA FSO link are discussed in section 5. The cascaded OA FSO link is first considered from a general system perspective, and then specific system implementations are shown. Finally, a conclusion is provided in section 6.

2 Channel statistics

Various probabilistic channel models representing the randomly varying signal intensity or channel loss have been used to describe atmospheric turbulence induced fading in the different turbulent regimes [1]. The GG distribution model is widely accepted for characterising the weak, moderate and strong turbulence conditions because results achieved match closely with experimental results [1, 9, 21]. The GG probability density function (pdf) is given as [1, 2, 6]

$$f_{GG}(h_t) = \frac{2(\alpha\beta)^{(\alpha+\beta)/2}}{\Gamma(\alpha)\Gamma(\beta)} h_t^{\left(\frac{\alpha+\beta}{2}\right)-1} K_{\alpha-\beta}\left(2\sqrt{\alpha\beta\, h_t}\right) \quad h_t > 0 \tag{1}$$

where α and β represents the number of large and small scale eddies due to the scattering process respectively, $\Gamma(.)$ is the Gamma function, $K_u(.)$ is the modified Bessel function of the second kind with order u and h_t describes the varying channel loss or gain due to atmospheric turbulence. h_t has a mean value of 1, and in the turbulent free limit, this mean value is attained at all times. With a plane wave assumption at the receiver, the parameters α and β are defined as [2]

$$\alpha = \left\{ \exp\left[\frac{0.49\,\sigma_R^2}{\left(1 + \left(1.11\,\sigma_R^{12/5}\right)\right)^{7/6}} \right] - 1 \right\}^{-1} \tag{2}$$

$$\beta = \left\{ \exp\left[\frac{0.51\,\sigma_R^2}{\left(1 + \left(0.69\,\sigma_R^{12/5}\right)\right)^{5/6}} \right] - 1 \right\}^{-1} \tag{3}$$

where σ_R^2, the Rytov variance used to characterise the different turbulence regimes is given as [2]

$$\sigma_R^2 = 1.23\, C_n^2 k^{7/6} D^{11/6} \tag{4}$$

where C_n^2 and D represents the refractive index structure parameter and the length of the FSO link respectively. The optical wave number $k = 2\pi/\lambda$ where λ is the optical wavelength [2]. Note that the

weak, moderate, strong and saturated turbulence regimes can be described by $\sigma_R^2 < 1$, $\sigma_R^2 \sim 1$, $\sigma_R^2 > 1$ and $\sigma_R^2 \to \infty$ respectively [2].

3 Single link optically preamplified FSO receiver model

Considering a direct detection scheme with NRZ-OOK modulation, an optically preamplified receiver model for a single link FSO communication system is shown in Fig. 1. The receiving lens (which couples the laser beam through a fibre into the OA) is assumed to be perfectly aligned with the transmitting lens and an optical band pass filter (OBPF) is used to reduce the amplified spontaneous emission (ASE) noise produced by optical amplification [2].

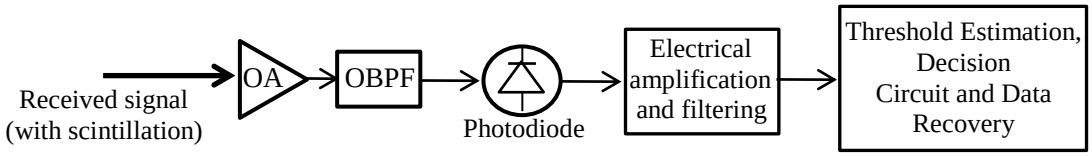

Fig. 1 Optically pre-amplified FSO receiver model.

After the filtering operation, a photodiode (PD) of responsivity $R = \eta q / h\nu$ where q is the electronic charge, η is the quantum efficiency, h is the Planck constant and ν is the frequency of the optical carrier is used for optical-to-electrical (O/E) conversion of the information-carrying signal followed by electrical amplification and filtering. A decision circuit (with a synchronisation subsystem) is then used to compare the received signal to a defined decision threshold and determine the transmitted data bit [2, 3].

3.1 Decision thresholding schemes

In a non-turbulent link, an optimal decision threshold is realistically achievable for a particular received power. However, the use of a non-adaptive decision threshold is not optimal in a turbulent link due to fluctuations in the signal levels [22]. To achieve an optimal performance in a turbulent link, an adaptive decision threshold that can constantly track the noise and signal levels is required

[8, 22] i.e. this is achievable if CSI is known. For example, this adaptive decision threshold can be obtained by using a Kalman filter [22]; which constantly tracks the variances and means of the bit level and updates the detection threshold thereby reducing the possibility of detection errors [22]. Laboratory experiments have shown that practically implementing the adaptive decision threshold for a given receiver is very challenging and time consuming due to the measurement precision and circuitry constraints required [23]. As a result of this difficulty, FSO link designers often prefer to make use of a non-adaptive decision threshold (based on a long term average received power) and include a link margin large enough to accommodate the turbulence induced scintillation [8].

3.1.1 Adaptive decision threshold

Now, considering a preamplified receiver system in a fading OOK FSO link where a Gaussian approximation (GA) is made for the noise in the received signal, the BER for a near optimal adaptive decision threshold, conditioned on h_t, is given as [2].

$$BER\left(P_{OAin_{av}}, h_t\right) = \frac{1}{2}\left[\operatorname{erfc}\left(\frac{Q\left(P_{OAin_{av}}, h_t\right)}{\sqrt{2}}\right)\right] \tag{5}$$

where the Q factor,

$$Q\left(P_{OAin_{av}}, h_t\right) = \frac{i_1\left(P_{OAin_{av}}, h_t\right) - i_0\left(P_{OAin_{av}}, h_t\right)}{\sigma_1\left(P_{OAin_{av}}, h_t\right) + \sigma_0\left(P_{OAin_{av}}, h_t\right)} \tag{6}$$

where the mean signal level at the sampling instant with OA input power P_{OAin_x}, $i_x = GRP_{OAin_x}$ for transmitted data bits, $x \in \{0,1\}$. This emerges from the binary symmetric channel assumption and there is a corresponding formula for the threshold which would be almost optimal if the noise was truly Gaussian. As NRZ-OOK signals are used, the power in a ONE $P_{OAin_1} = \frac{2r}{r+1} P_{OAin_{av}}$, the power

in a ZERO $P_{OAin_0} = \frac{2}{r+1} P_{OAin_{av}}$ where $r = P_{OAin_1} / P_{OAin_0}$ is the extinction ratio, $P_{OAin_{av}}$ is the average power at the OA input (i.e. the average power over the data stream when $h_t = 1$) and G is the gain (can be either fixed or saturated depending on $P_{OAin_{av}}$) of the OA. The total noise current variance $\sigma_x^2 = \sigma_{sx-sp}^2 + \sigma_{sp-sp}^2 + \sigma_{sh,x}^2 + \sigma_{th}^2$ where the signal-spontaneous beat noise $\sigma_{sx-sp}^2 = 4GR^2 P_{OAin_x} N_0 B_e$, the shot noise $\sigma_{sh,x}^2 = 2qR(GP_{OAin_x} + m_t N_0 B_{opt}) B_e$ and the spontaneous-spontaneous beat noise $\sigma_{sp-sp}^2 = 2m_t R^2 N_0^2 B_{opt} B_e \left(1 - \frac{B_e}{2B_{opt}}\right)$. σ_{th}^2 is the receiver thermal noise variance, B_{opt} is the OBPF bandwidth, m_t is the number of polarisation states parameter (1 or 2) and $B_e = 0.7R_b$ is the receiver noise equivalent bandwidth where R_b is the bit rate. The ASE noise is described by its power spectral density (PSD) $N_0 = \frac{1}{2}(NFG - 1)hv$ where NF is the noise figure [2].

3.1.2 Saturated OA mitigation of turbulence with non-adaptive decision threshold

The idea of using OAs for the suppression of turbulence induced scintillation is based on exploiting the OA's gain saturation characteristics under the assumption of appropriately fast gain dynamics relative to turbulence. This assumption is valid since a SOA and a erbium-doped fibre amplifier (EDFA) have gain recovery dynamics of around 10 GHz and 5 kHz respectively while turbulence fluctuations are around 1 kHz [2, 15, 24]. The OA gain G is implicitly related to the instantaneous optical signal power at the OA input P_{in} as shown below [18]

$$P_{in} = \frac{P_{sat}}{G-1} \ln\left(\frac{G_{ss}}{G}\right) \tag{7}$$

where $P_{in} = P_{OAin_{av}} h_t$, and where G_{ss} and P_{sat} are the small signal (fixed) gain and the internal saturation power of the OA respectively. Note that $G \to G_{ss}$ when $\frac{P_{in}}{P_{sat}} \to 0$. As shown in (7), the

OA is able to adjust its gain to new power levels by providing higher gains to lower input powers and lower gains to higher input powers thereby allowing for its use in scintillation suppression. This essentially instantaneous equalization property of the saturated OA results in more stable average output power (reduced fluctuations) and thus, an optical receiver with a non-adaptive decision threshold can be straightforwardly deployed when an optical preamplifier placed after the turbulent link can nevertheless be driven into saturation [15]. The optical signal power at the output of the OA is obtained as

$$P_{out}\left(P_{in}\right) = G\left(P_{in}\right)P_{in} \tag{8}$$

Now, the non-adaptive decision threshold, assumed set to a long term average received power at the photodiode, can be obtained by statistically averaging (8) over the atmospheric turbulence pdf and it is obtained as

$$i_D\left(P_{OAin_{av}}\right) = R\int_0^{\infty} P_{out}\left(P_{OAin_{av}} h_t\right) f_{GG}\left(h_t\right) dh_t \tag{9}$$

It is stressed that the treatment here is restricted to a single wavelength system. Multiple wavelengths constitute a natural further development of this work. Under such circumstances, assuming that an OA is not to favour particular wavelength channels systematically, it will be necessary to ensure gain flatness at least in the small signal regime. Furthermore to continue to benefit from the turbulence mitigation discussed in this single wavelength case whilst avoiding gain crosstalk it is necessary to ensure that individual channels saturate independently. This will be harder to achieve with an SOA (homogeneously broadened) than with an EDFA (inhomogeneously broadened). In choosing a gain flat EDFA for such a system (e.g. [25-27]), it remains necessary to ensure the gain dynamics are fast enough to track atmospheric fluctuations.

3.2 Single link BER analysis

The BER is the key performance attribute commonly used for FSO communication systems analysis [18]. By making a GA assumption for the noise, a BER, conditioned on the instantaneous loss (or gain) state of the turbulent channel h_t, is given as [28]

$$BER\left(P_{OAin_{av}}, h_t\right) = \frac{1}{2}\left[\frac{1}{2}\operatorname{erfc}\left(\frac{i_D - i_0\left(P_{OAin_{av}}, h_t\right)}{\sqrt{2\sigma_0^2\left(P_{OAin_{av}}, h_t\right)}}\right) + \frac{1}{2}\operatorname{erfc}\left(\frac{i_1\left(P_{OAin_{av}}, h_t\right) - i_D}{\sqrt{2\sigma_1^2\left(P_{OAin_{av}}, h_t\right)}}\right)\right] \tag{10}$$

The value of i_D in (10) can be defined in such a way as to justify the use of Q and adaptive thresholding (and hence equation (5)) or by (9) in the non-adaptive thresholding case. In the adaptive case it varies with h_t, in the case of (9) it does not vary with h_t. Now the average BER obtained by statistically averaging the conditioned BER over the turbulence PDF is given as [2]

$$BER_{av}\left(P_{OAin_{av}}\right) = \int_0^\infty BER\left(P_{OAin_{av}}, h_t\right) f_{GG}(h_t)\, dh_t \tag{11}$$

For a non-amplified receiver system, $G = 1$, $N_0 = 0$ and then the receiver thermal noise is the dominant impairment (i.e. $\sigma_0 = \sigma_1 = \sigma_{th}$) [18].

4 Cascaded OA FSO communication system

Fig. 2 shows a cascaded OA FSO communication system model. In a cascaded OA FSO link (and also often in conventional optically preamplified receiver), the basic receiver sensitivity at the PD input becomes less useful in evaluating system performance due to the accumulation of ASE noise. It is therefore necessary to determine the optical power and the ASE noise at each OA stage. When these two quantities are known, the optical signal to noise ratio (OSNR), which can be related to the BER [18] is then obtainable. Due to the random effect of atmospheric turbulence, analytical methods are stretched by multiple links when used. Therefore, Monte Carlo (MC) simulation techniques are

used here to model the cascaded OA FSO communication system. By using MC methods, random samples of the power fluctuation due to atmospheric turbulence can be determined for each section of the cascade and used to obtain the accumulated power, ASE noise and OSNR pdfs at each OA stage. Each interamplifier section is assumed statistically independent in its turbulence.

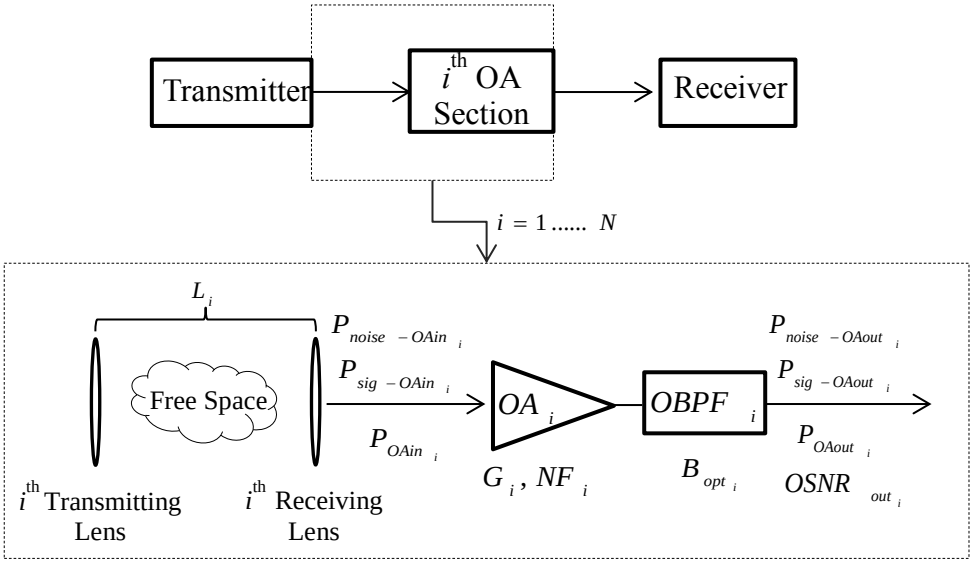

Fig. 2 A cascaded OA FSO communication system model.

With the assumption of a clean atmosphere, the total loss in each interamplifier section of the link $L_i = L_{nt_i} h_{GG_i}$ $(i = 1 \ldots\ldots N)$ where h_{GG_i} is the GG random variable describing the fluctuations due to atmospheric turbulence before the ith OA and N is the total number of OAs in the cascade. L_{nt_i} is the turbulence-free fixed path loss (< 1) (i.e. defined by the attenuation due to geometric spread and atmospheric propagation [8]) and it is given as [29]

$$L_{nt} = \left(\frac{d_{rx}}{\phi D} \right)^2 \alpha \tag{12}$$

where d_{rx} and ϕ represents the receiving lens diameter and beam divergence angle respectively. $\alpha = e^{-\beta D}$ is the atmospheric attenuation in each interamplifier section of the link where β represents

the attenuation coefficients due to absorption and scattering [30]. The total power at the input of the ith OA is given as

$$P_{OAin_i} = P_{sig-OAin_i} + P_{noise-OAin_i} \tag{13}$$

The signal power at the input of the ith OA is given as

$$P_{sig-OAin_i} = P_{sig-OAout_i} L_i \qquad (i = 2 \ldots\ldots N) \tag{14}$$

For the first OA, $P_{sig-OAin_1} = P_{TX} L_1$. Also, the ASE power at the input of the ith OA is given as

$$P_{noise-OAin_i} = m_t B_{opt} N_{0-OAin_i} \tag{15}$$

The ASE PSD at the input of the ith OA is given as

$$N_{o-OAin_i} = N_{o-OAout_{i-1}} L_i \qquad (i = 2 \ldots\ldots N) \tag{16}$$

For the first OA, $N_{o-OAin_1} = 0$. At the ith OA, the self ASE PSD is given as

$$N_{o-OA_i} = \frac{1}{2}\left(NFG_i\left(P_{OAin_i}\right) - 1\right)h\nu \qquad (i = 1 \ldots\ldots N) \tag{17}$$

The self ASE power is given as

$$P_{noise-OA_i}\left(P_{OAin_i}\right) = m_t B_{opt} N_{0-OA_i} \tag{18}$$

After amplifying the optical signal with a gain $G_i\left(P_{OAin_i}\right)$, the signal power at the output of the ith OA is given as

$$P_{sig-OAout_i}\left(P_{sig-OAin_i}, P_{noise-OAin_i}\right) = G_i\left(P_{sig-OAin_i} + P_{noise-OAin_i}\right)P_{sig-OAin_i} \qquad (i = 1 \ldots\ldots N) \tag{19}$$

The ASE power at the output of the ith OA is given as

$$P_{noise\ -OAout\ _i}\left(P_{sig\ -OAin\ _i}, P_{noise\ -OAin\ _i}\right) = G_i\left(P_{sig\ -OAin\ _i} + P_{noise\ -OAin\ _i}\right)P_{noise\ -OAin\ _i} + P_{noise\ -OA_i}\left(P_{OAin\ _i}\right) \quad (20)$$

The ASE PSD at the output of the ith OA is given as

$$N_{o-OAout\ _i} = N_{o-OAin\ _i} G_i + N_{o-OA_i} \qquad (i = 1 \ldots \ldots N) \quad (21)$$

The total power at the output of the ith OA is given as

$$P_{OAout\ _i} = P_{sig\ -OAout\ _i} + P_{noise\ -OAout\ _i} \quad (22)$$

Now, the OSNR at the output of the ith OA is given as

$$OSNR_{\ out\ _i}\left(P_{sig\ -OAin\ _i}, P_{noise\ -OAin\ _i}\right) = \frac{P_{sig\ -OAout\ _i}\left(P_{sig\ -OAin\ _i}, P_{noise\ -OAin\ _i}\right)}{P_{noise\ -OAout\ _i}\left(P_{sig\ -OAin\ _i}, P_{noise\ -OAin\ _i}\right)} \quad (i = 1 \ldots \ldots N) \quad (23)$$

Note that here the OSNR is defined over B_{opt} rather than a standardised bandwidth (such as 12.5 GHz) as is sometimes the practice.

4.1 Cascaded OA BER analysis

By adapting (10) from the single OA case and including (23), the BER immediately after the ith OA section is derived as

$$BER_{\ i} = \frac{1}{2}\left[\frac{1}{2}\operatorname{erfc}\left(\frac{A_{0_i} OSNR_{\ out\ _i}}{\sqrt{BOSNR_{\ out\ _i} + C + D_i OSNR^{\ 2}_{\ out\ _i}}}\right) + \frac{1}{2}\operatorname{erfc}\left(\frac{A_{1_i} OSNR_{\ out\ _i}}{\sqrt{BrOSNR_{\ out\ _i} + C + D_i OSNR^{\ 2}_{\ out\ _i}}}\right)\right] \quad (24)$$

where $A_{0_i} = \frac{i_{D_i}(r+1) - 2RP_{sig\ -OAout\ _i}}{2RP_{sig\ -OAout\ _i}(r+1)}$, $A_{1_i} = \frac{2rRP_{sig\ -OAout\ _i} - i_{D_i}(r+1)}{2RP_{sig\ -OAout\ _i}(r+1)}$ and i_{D_i} value depends on the decision thresholding scheme used at the receiver, $B = \frac{4B_e}{(r+1)m_t B_{opt}}$, $C = \frac{B_e(2B_{opt} - Be)}{2m_t B^2_{opt}}$ and

$D_i = \frac{\sigma_{th}^2}{2R^2 P_{sig-OAout_i}^2}$. An equivalent approach is used for the adaptive case when going directly to Q as in equation (5).

5 Results and Discussion

The parameters used for the numerical analysis and MC simulations are shown in Tables 1, 2 and 3. The MC simulation allows the OA gain to respond freely, using complete saturation characteristic and incorporating the effect of ASE noise on the saturated operation. For the purpose of this analysis, an OA that can be driven into gain saturation (P_{sat} = 5 dBm) is referred to as a saturated gain OA and an OA that cannot be driven into gain saturation ($P_{sat} \rightarrow \infty$) is referred to as a fixed gain OA. A baseline (unimpaired) receiver sensitivity of -23 dBm corresponding to a BER of 10^{-12} is used to obtain the receiver thermal noise (i.e. 7×10^{-7} A) [2].

Table 1 Parameters used for the numerical analysis and MC simulations

Parameter	Symbol	Value
Optical wavelength	λ	1550 nm
Bit rate	R_b	2.5 Gb/s
Transmitted optical power	P_T	20 dBm
OA small signal gain	G_{ss}	25 dB
OBPF bandwidth	B_{opt}	70 GHz
Noise figure	NF	5 dB
Quantum efficiency	η	1
Extinction ratio	r	10 dB

5.1 Single FSO Link

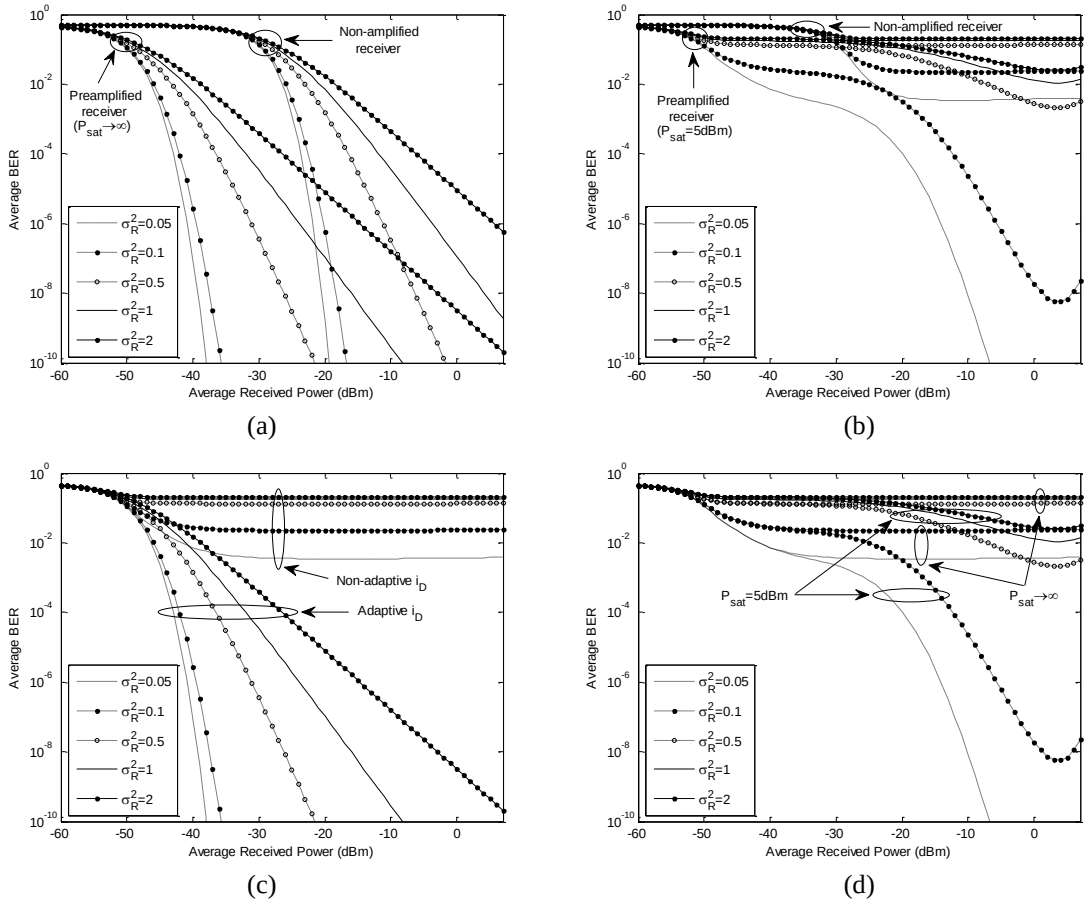

Fig. 3 Average BER against average received power for different turbulence regimes in a single FSO link.
a Non-amplified receiver and fixed gain preamplified receiver - Adaptive decision threshold
b Non-amplified receiver and saturated gain preamplified receiver – Non-adaptive decision threshold
c Adaptive and non-adaptive decision threshold - Fixed gain preamplified receiver
d Fixed and saturated gain preamplified receiver - Non-adaptive decision threshold

Fig. 3 shows the BER curves for different turbulence regimes in a single FSO link. In Fig. 3a, the advantage of including a preamplifier at the receiver is shown as the BER curves for a fixed gain preamplified receiver and a non-amplified receiver has a power difference of around 18 dB at a target BER of 10^{-10}. When a non-adaptive decision threshold is used in Fig. 3b, a non-amplified receiver gives BER floors at high (poor) BER values ($> 10^{-3}$) in all turbulence regimes because unlike the adaptive decision threshold in Fig. 3a, a non-adaptive decision threshold does not properly take the power fluctuations caused by atmospheric turbulence into consideration. However, when a saturated gain preamplifier is used at the receiver, low BER values ($< 10^{-8}$ for $\sigma_R^2 = 0.1$) are obtained because

a saturated gain preamplifier suppresses scintillation by adjusting its gain to the fluctuating power levels. A comparison of the BER curves for a fixed gain preamplified receiver with a non-adaptive decision threshold in Fig. 3c and Fig. 3b shows a consistent power difference of around 20 dB across all turbulence regimes but BER floors at high BER values ($> 10^{-3}$) were obtained in both cases across all turbulence regimes. This shows that a fixed gain preamplifier can be used to improve receiver sensitivity but it cannot suppress scintillation. As mentioned in [15, 16] and shown in Fig. 3b and 3d, the BER performance of a saturated gain preamplified receiver reaches an optimal level when the power at the preamplifier input is comparable to its P_{sat} value. For instance, the BER curve (σ_R^2 = 0.1) for a saturated gain preamplified receiver in Fig. 3b reaches an optimal value at an average received power of around 5dBm; which is the P_{sat} value of the preamplifier. While there is no fundamental reason not to operate optical preamplifiers in the saturation regime, an optical preamplifier with a high P_{sat} value would only be driven into gain saturation if the input power is also high. If a high input power is required to drive the preamplifier into gain saturation, the power at the preamplifier output may have to be reduced (i.e. by introducing an optical fibre and additional attenuation) before it arrives at the receiver because high powers can eventually overload the receiver. Alternatively, preamplifier gain saturation can be achieved with a low power if the P_{sat} value of the preamplifier is also low thereby avoiding the possibility of overloading the receiver.

To summarize, in a turbulent atmosphere, amplifier saturation does not improve receiver sensitivity when an adaptive decision threshold is used at the receiver. This is because the adaptive threshold mitigates the scintillation impact, leaving saturation to be a signal power impairment. Saturation is primarily helpful in the preamplifier when a (less complex) non-adaptive decision threshold is used at the receiver. This threshold benefits from a stable input power to the photodiode caused by saturation providing higher gains to lower amplifier input powers and lower gains to higher amplifier input powers. Thus the argument for introducing a saturated amplifier, versus having no amplifier at

all, is that the saturation mitigates the significant sensitivity impairment caused by the atmospheric scintillations. It also shows improvement when compared to an otherwise identical non-saturating amplifier since a saturated amplifier is able to provide some scintillation suppression.

5.2 Cascaded OA FSO Link

The parameters required for the design of each interamplifier section of a cascaded OA FSO link are shown in Table 2. Since all these design parameters can be represented by the σ_R^2 and L_{nt} per section [2, 29] as shown in equations (4) and (12), fixed σ_R^2 and L_{nt} values per section are used for the analysis. Having these two fixed values is manageable and ensures the possibility of mapping results into a variety of practical realizations. Therefore, for each interamplifier section of the cascaded OA FSO link, a general system perspective is taken and how a specific implementation will achieve the fixed parameters is not specified. This should inform understanding of section 5.2.1. However, the mapping is then performed in section 5.2.2 by defining specific values for the physical design parameters.

Table 2 Design parameters required for a FSO link

Design Parameter	Symbol
Receiving lens diameter	d_{rx}
Beam divergence angle	ϕ
Link length	D
Refractive index structure constant	C_n^2

5.2.1 A General System Perspective

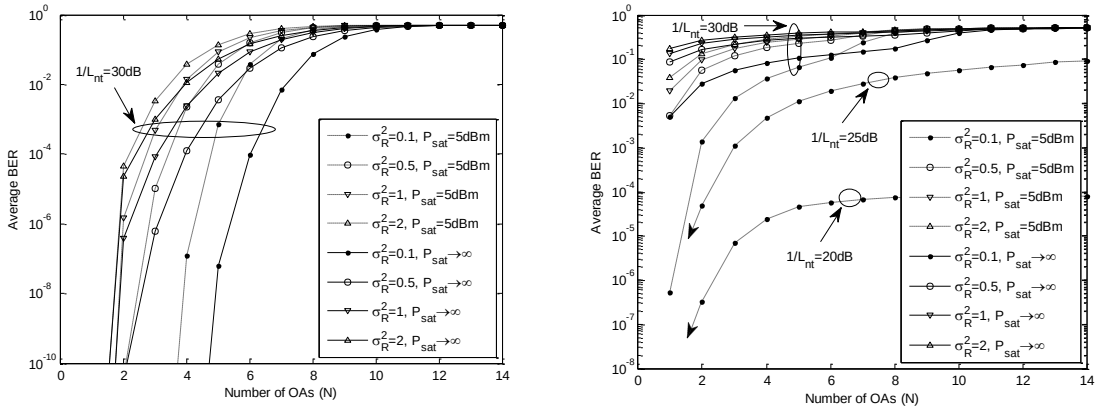

(a) (b)

Fig. 5 Average BER at different OA positions in a cascaded OA FSO link. Arrow indicates that the next data point is effectively zero.
a Adaptive decision threshold
b Non-adaptive decision threshold

Fig. 5 shows BER results at different OA positions in a cascaded OA FSO link. In Fig. 5a, it is shown that when $\sigma_R^2 = 0.1$, a BER value less than 10^{-10} is achievable at the 4th and 3th OA position in the cascade when a fixed and saturated gain OA cascade is used respectively. This shows that when an adaptive decision threshold is used at the receiver, a fixed gain OA cascade performs better than a saturated gain OA cascade because while the OA gain remains constant (i.e. G_{ss}) in a fixed gain OA cascade, it decreases ($< G_{ss}$) in a saturated gain OA cascade. In Fig. 5b where a non-adaptive decision threshold is used at the receiver, high BER values ($> 10^{-3}$) are obtained in all turbulence regimes for a fixed gain OA cascade but low BER values ($< 10^{-6}$ when $\sigma_R^2 = 0.1$) can be obtained at the first OA position in a saturated gain OA cascade. In Fig. 5a and 5b, the BER curves for the fixed and saturated gain OA cascades are shown to converge after the 9th OA position because since $G_{ss} < 1/L_{nt}$, the powers at the input of the OAs in the saturated gain OA cascade ultimately becomes insufficient to drive the OAs into saturation making the performance similar to a fixed gain OA cascade that has net loss. Note that the overall BER performance can be improved using OAs with higher G_{ss} values,

reducing the turbulence-free fixed path loss in each interamplifier section of the link as shown in Fig. 5b or by applying an appropriate forward error correction (FEC) technique with interleaving [2, 10].

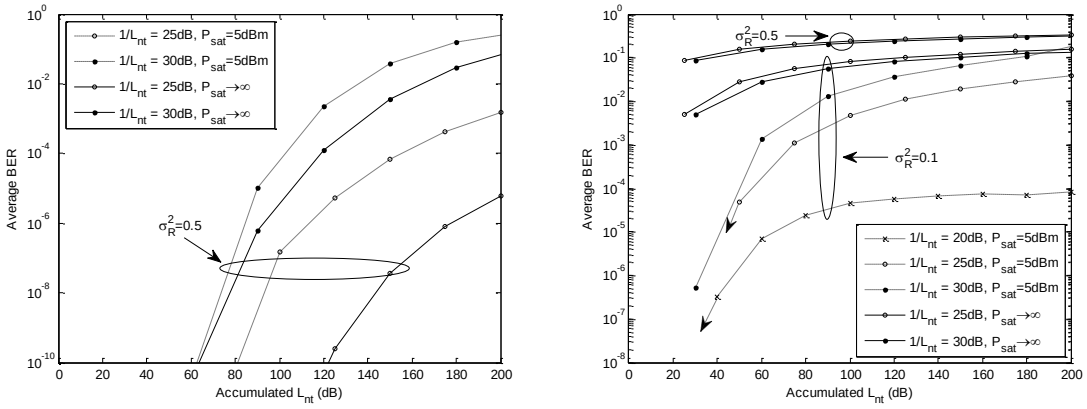

(a) (b)

Fig. 6 Average BER against accumulated L_{nt} in a cascaded OA FSO link. Arrows indicate that the next data point is effectively zero.
a Adaptive decision threshold
b Non-adaptive decision threshold

Fig. 6 shows the BER curves for a cascaded OA FSO link. The data points occur at integer multiples of the section losses i.e. as we move rightwards the number of OAs increases at each data point. In Fig. 6a where an adaptive threshold is used at the receiver, the BER performances are shown to perform better when the number of OAs in the cascade is increased (i.e. reduced L_{nt} per interamplifier section). Also, the BER performance ($1/L_{nt}$ = 25dB) for a fixed gain OA cascade is seen to outperform a saturated gain OA cascade by around 40 dB at a target BER of 10^{-10}. In Fig. 6a and 6b, the BER curves (σ_R^2 = 0.5) for a saturated gain OA cascade show that an adaptive decision threshold outperforms a non-adaptive decision threshold, however, an improved performance is noticed for the non-adaptive decision threshold when σ_R^2 = 0.1. Even though Fig. 6 (b) does not show very low BER values, it clearly shows improved performances when a saturated gain OA cascade is used and the lower BER results obtained when $1/L_{nt}$ = 20dB show that frequent low gain saturated amplification

can keep the fades down to a manageable level. Naturally still more frequent saturated amplification can lead to further improvement.

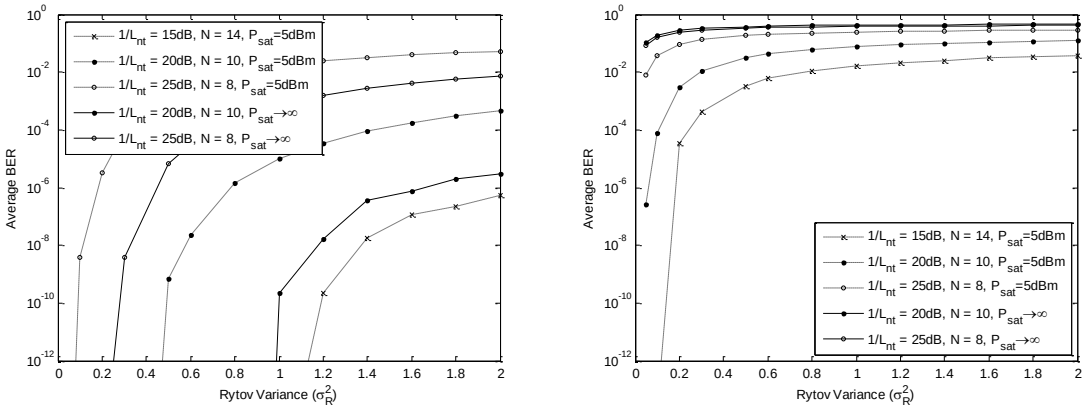

(a) (b)

Fig. 7 Average BER against per OA section Rytov variance in a cascaded OA FSO link. Arrows indicate that the next data point is effectively zero.
a Adaptive decision threshold
b Non-adaptive decision threshold

Fig. 7 shows the BER curves for different accumulated L_{nt} values in a cascaded OA FSO link. The values chosen are such as to give approximately the same overall accumulated system loss (8×25=200 dB, 10×20=200 dB, 14×15=210 dB). In Fig. 7a, the BER curves obtained for a fixed gain OA cascade shows that a BER of 10^{-12} is obtained at around σ_R^2 = 0.98 and σ_R^2 = 0.26 when 10 and 8 OAs are used respectively. For a saturated gain OA cascade, a BER of 10^{-12} is obtained at around σ_R^2 = 1.12, σ_R^2 = 0.44 and σ_R^2 = 0.09 when 14, 10 and 8 OAs are used respectively. While this further indicates that a fixed gain OA cascade performs better than a saturated gain OA cascade when an adaptive decision threshold is used at the receiver, the reverse is the case in Fig. 7b where a non-adaptive decision threshold is used at the receiver as a saturated OA cascade is shown to perform better because the BER curve obtained for a saturated gain OA cascade shows that a BER of 10^{-12} is obtained at around σ_R^2 = 0.1 when 14 OAs are used while high BER values ($> 10^{-2}$) are obtained regardless of the number of OA used for a fixed gain OA cascade.

5.2.2 Specific System Implementation

As earlier mentioned in section 5.2 and shown in Table 2, the defined L_{nt} and σ_R^2 per section (i.e. single FSO link) can be mapped into a variety of specific per section design parameters. In Table 3, when $1/L_{nt}$ = 35dB and σ_R^2 = 0.1 (i.e. design B), the achievable communication distance of each interamplifier section of the cascaded OA FSO link is 2.230km.

Table 3 Mapping L_{nt} and σ_R^2 per section into specific design parameters

Design	A	B	C	D	E	F
$1/L_{nt}$ (dB)	35	35	30	30	25	20
σ_R^2	0.5	0.1	0.5	0.1	0.1	0.1
d_{rx} (m)	4×10^{-2}	7×10^{-2}	3.5×10^{-2}	4×10^{-2}	9×10^{-2}	5×10^{-2}
ϕ (rad)	1×10^{-3}	1.7×10^{-3}	8.5×10^{-4}	1×10^{-3}	2.5×10^{-3}	1.5×10^{-3}
C_n^2 ($m^{-2/3}$)	6.1×10^{-15}	1.2×10^{-15}	1.6×10^{-14}	3.4×10^{-15}	1.2×10^{-14}	3.8×10^{-14}
D (m)	2168	2230	1274	1239	633	331

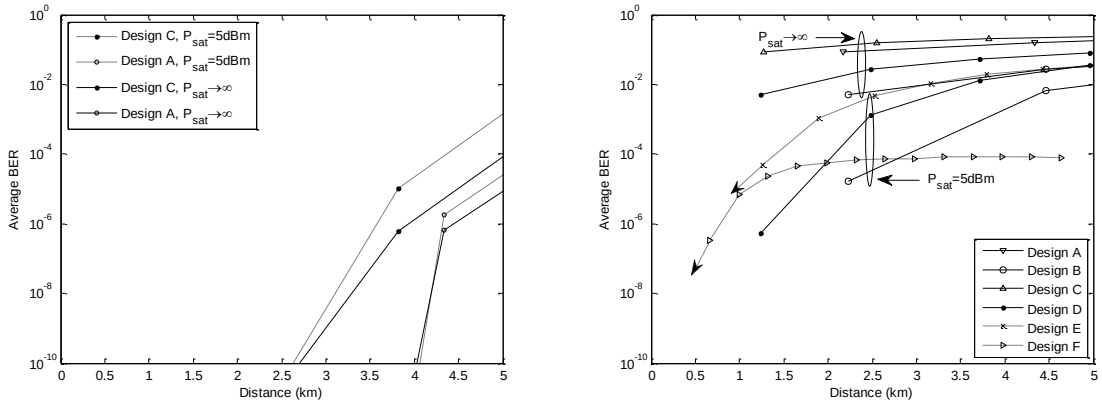

(a) (b)

Fig. 8 Average BER against distance in a cascaded OA FSO link. Arrows indicate that the next data point is effectively zero.
a Adaptive decision threshold
b Non-adaptive decision threshold

The BER curves in Fig. 8 shows the possibility of extending reach in FSO communication systems with an OA cascade while assuming the use of the design parameters in Table 3. In Fig. 8a where an adaptive decision threshold is used in design A, a BER of 10^{-10} is achievable at an overall distance

of about 4km (with N = 2) in both fixed and saturated gain OA cascades. In design C, the achievable distance reduces to about 2.5km (with N = 2) in both fixed and saturated gain OA cascades. The achievable distance of design C relative to design A reduces because communication over shorter distances naturally results in lower turbulence-free fixed path loss values. In Fig. 8b where a non-adaptive decision threshold is used, the BER curves obtained show that the optical signal is able to travel for longer distances at lower BER values along an OA cascade with saturated gain OAs than with fixed gain OAs. At 2.5km, design D is able to achieve lower BER values ($< 10^{-2}$) with saturated gain OAs compared to using fixed gain OAs ($> 10^{-2}$). Also, it is shown in Fig. 8b that increasing the number of OAs (i.e. reducing $1/L_{nt}$) yields improved BER performances. For instance, design F is able to achieve a BER of around 10^{-4} while design E achieved a higher BER value ($\approx 10^{-2}$) at a distance of 5km. Ultimately, the overall BER performance can be improved by using an OA with a higher small signal gain value or reducing the distance of each interamplifier section of the cascaded OA FSO link.

6 Conclusion

This paper examines the performance of a FSO communication system in a turbulent atmosphere employing an OA cascade to extend reach by applying numerical and MC simulation techniques. Performance modelling in the presence of ASE noise is shown. The use of a saturated gain OA at the receiver is investigated and the BER results obtained for the single and cascaded OA FSO links show its ability to suppress scintillation when CSI is not known and a non-adaptive decision threshold is used. The presented results also show that an OA cascade can be successfully used to extend reach in FSO communication systems. Even though the results presented show that the performance of an adaptive decision threshold is superior to a non-adaptive decision threshold (especially in higher turbulence regimes) for both saturated and fixed gain preamplified receivers, its practical implementation is far more complicated and costly. It has also been shown that in a turbulent

atmosphere, saturation is primarily helpful in the preamplifier when a non-adaptive decision threshold is used at the receiver. Therefore the use of a non-adaptive decision threshold with a saturated gain preamplified receiver is recommended for scintillation suppression in FSO communication systems since good performance is achievable without the need of further complexity in the circuitry and processing.

7 References

[1] L. C. Andrews and R. L. Phillips, *Laser Beam Propagation Through Random Media*: Society of Photo Optical, 2005.

[2] A. O. Aladeloba, A. J. Phillips, and M. S. Woolfson, "Improved bit error rate evaluation for optically pre-amplified free-space optical communication systems in turbulent atmosphere," *IET Optoelectronics,,* vol. 6, pp. 26-33, 2012.

[3] M. Razavi and J. H. Shapiro, "Wireless optical communications via diversity reception and optical preamplification," in *IEEE International Conference on Communications, 2003. ICC '03.* , 2003, pp. 2262-2266 vol.3.

[4] T. H. Carbonneau and D. R. Wisely, "Opportunities and challenges for optical wireless: the competitive advantage of free space telecommunications links in today's crowded marketplace," 1998, pp. 119-128.

[5] D. Kedar and S. Arnon, "Urban optical wireless communication networks: the main challenges and possible solutions," *Communications Magazine, IEEE,* vol. 42, pp. S2-S7, 2004.

[6] Z. Xiaoming and J. M. Kahn, "Free-space optical communication through atmospheric turbulence channels," *IEEE Transactions on Communications,,* vol. 50, pp. 1293-1300, 2002.

[7] W. O. Popoola, Z. Ghassemlooy, J. I. H. Allen, E. Leitgeb, and S. Gao, "Free-space optical communication employing subcarrier modulation and spatial diversity in atmospheric turbulence channel," *IET Optoelectronics,,* vol. 2, pp. 16-23, 2008.

[8] Z. Ghassemlooy, W. O. Popoola, and S. Rajbhandari, *Optical Wireless Communications: System and Channel Modelling with MATLAB*. Boca Raton, FL 33487-2742, 2013.

[9] M. Khalighi, N. Schwartz, N. Aitamer, and S. Bourennane, "Fading Reduction by Aperture Averaging and Spatial Diversity in Optical Wireless Systems," *IEEE/OSA Journal of Optical Communications and Networking,,* vol. 1, pp. 580-593, 2009.

[10] Z. Xiaoming and J. M. Kahn, "Performance bounds for coded free-space optical communications through atmospheric turbulence channels," *IEEE Transactions on Communications,,* vol. 51, pp. 1233-1239, 2003.

[11] S. M. Navidpour, M. Uysal, and M. Kavehrad, "BER Performance of Free-Space Optical Transmission with Spatial Diversity," *IEEE Transactions on Wireless Communications,,* vol. 6, pp. 2813-2819, 2007.

[12] S. G. Wilson, M. Brandt-Pearce, C. Qianling, and J. H. Leveque, III, "Free-Space Optical MIMO Transmission With Q-ary PPM," *IEEE Transactions on Communications,,* vol. 53, pp. 1402-1412, 2005.

[13] M. Safari and M. Uysal, "Relay-Assisted Free-Space Optical Communication," in *Conference Record of the Forty-First Asilomar Conference on Signals, Systems and Computers, 2007. ACSSC 2007.* , 2007, pp. 1891-1895.

[14] Z. Xiaoming and J. M. Kahn, "Markov chain model in maximum-likelihood sequence detection for free-space optical communication through atmospheric turbulence channels," *IEEE Transactions on Communications,,* vol. 51, pp. 509-516, 2003.

[15] K. Yiannopoulos, N. C. Sagias, and A. C. Boucouvalas, "Fade Mitigation Based on Semiconductor Optical Amplifiers," *Journal of Lightwave Technology,,* vol. 31, pp. 3621-3630, 2013.
[16] A. C. Boucouvalas, N. C. Sagias, and K. Yiannopoulos, "First order statistics of semiconductor optical amplifier assisted optical wireless systems under log-normal fading," in *2nd International Workshop on Optical Wireless Communications (IWOW), 2013* 2013, pp. 142-146.
[17] M. Abtahi, P. Lemieux, W. Mathlouthi, and L. A. Rusch, "Suppression of Turbulence-Induced Scintillation in Free-Space Optical Communication Systems Using Saturated Optical Amplifiers," *Journal of Lightwave Technology, ,* vol. 24, pp. 4966-4973, 2006.
[18] R. Ramaswami, K. Sivarajan, and G. Sasaki, *Optical Networks: A Practical Perspective, 3rd Edition*: Morgan Kaufmann Publishers Inc., 2009.
[19] E. Ciaramella, Y. Arimoto, G. Contestabile, M. Presi, A. D'Errico, V. Guarino*, et al.*, "1.28 terabit/s (32x40 Gbit/s) wdm transmission system for free space optical communications," *IEEE Journal on Selected Areas in Communications,,* vol. 27, pp. 1639-1645, 2009.
[20] N. C. Sagias, K. Yiannopoulos, and A. C. Boucouvalas, "Bit-error-rate performance of semiconductor optical amplifiers in negative exponential fading," in *Computer Aided Modeling and Design of Communication Links and Networks (CAMAD), 2014 IEEE 19th International Workshop on*, 2014, pp. 168-172.
[21] A. K. Majumdar, "Free-space laser communication performance in the atmospheric channel," *Journal of Optical and Fiber Communications Reports,* vol. 2, pp. 345-396, 2005/10/01 2005.
[22] H. R. Burris, A. E. Reed, N. M. Namazi, W. J. Scharpf, M. J. Vicheck, M. F. Stell*, et al.*, "Adaptive thresholding for free-space optical communication receivers with multiplicative noise," in *Aerospace Conference Proceedings, 2002. IEEE*, 2002, pp. 3-1473-3-1480 vol.3.
[23] H. R. Burris, C. I. Moore, L. A. Swingen, L. M. Wasiczko, R. Mahon, M. F. Stell*, et al.*, "Laboratory implementation of an adaptive thresholding system for free-space optical communication receivers with signal dependent noise," in *Optics & Photonics 2005*, 2005, pp. 58920W-58920W-20.
[24] C. R. Giles, J. R. Simpson, and E. Desurvire, "Transient gain and cross talk in erbium-doped fiber amplifiers," *Optics Letters,* vol. 14, pp. 880-882, 1989/08/15 1989.
[25] S. Singh and R. Kaler, "Performance optimization of EDFA–Raman hybrid optical amplifier using genetic algorithm," *Optics & Laser Technology,* vol. 68, pp. 89-95, 2015.
[26] S. Singh and R. Kaler, "Novel optical flat-gain hybrid amplifier for dense wavelength division multiplexed system," *Photonics Technology Letters, IEEE,* vol. 26, pp. 173-176, 2014.
[27] S. Singh and R. Kaler, "Flat-gain L-band Raman-EDFA hybrid optical amplifier for dense wavelength division multiplexed system," *Photonics Technology Letters, IEEE,* vol. 25, pp. 250-252, 2013.
[28] L. F. B. Ribeiro, J. Da Rocha, and J. L. Pinto, "Performance evaluation of EDFA preamplified receivers taking into account intersymbol interference," *Journal of Lightwave Technology,* vol. 13, pp. 225-232, 1995.
[29] A. O. Aladeloba, M. S. Woolfson, and A. J. Phillips, "WDM FSO network with turbulence-accentuated interchannel crosstalk," *Optical Communications and Networking, IEEE/OSA Journal of,* vol. 5, pp. 641-651, 2013.
[30] J. Akella, M. Yuksel, and S. Kalyanaraman, "Error analysis of multi-hop free-space optical communication," in *IEEE International Conference on Communications, 2005. ICC 2005,*, 2005, pp. 1777-1781 Vol. 3.